

## STABILITY CHARACTERISTICS OF THE 500 MW INDIAN PFBR

by

**Vijayan L. ANURAJ\***, **Goverapet S. SRINIVASAN**, and **Kunhiraman DEVAN**

Indira Gandhi Centre for Atomic Research Kalpakkam, Tamil Nadu, India

Scientific paper  
DOI: 10.2298/NTRP1502113A

After the successful operation of the fast breeder test reactor for over two decades, India is now nearing the completion of a 500 MW (electrical) prototype fast breeder reactor. This commercial scale power reactor is a sodium-cooled, pool-type, mixed-oxide fuelled fast reactor. The stability characteristics of the reactor are an important safety aspect to be studied. In the present work, linear stability of the prototype fast breeder reactor analysis is carried out using the transfer function method, while the stability of the system is checked via the Nyquist criteria. For the completeness of the study, transient analysis with various kinds of reactivity perturbations was carried out. The response of the system in both cases indicated that the system is stable.

*Key words:* liquid metal fast breeder reactor; linear stability; prototype fast breeder reactor; Nyquist plot

### INTRODUCTION

In its second stage, India's three-stage nuclear program involves sodium-cooled fast reactors. The plutonium required for these reactors is produced by pressurized heavy water reactors (PHWR) of the first stage, in operation for many years. India's first fast reactor (FBTR), a test reactor with a power rate of 40 MW (thermal) has been in operation at Kalpakkam since 1985. Based on the operating experience of the FBTR spanning over two decades, a commercial scale prototype reactor, prototype fast breeder reactor (PFBR), has been designed and is in the final stages of construction. The neutronic stability of a reactor ensuring safe operation necessitates the development of a computational tool for the stability analysis of such reactors. With this in mind, a mathematical model and a computer program (FORTRAN) based on the said model have been developed at the Indira Gandhi Centre for Atomic Research.

PFBR linear stability analysis using transfer functions and the Nyquist criteria is performed using the newly developed program. Even though linear stability analysis ensures the stability of such a tightly coupled reactor core, a study taking into consideration real-time transient analysis is done for various reactivity perturbations via a detailed model of feedbacks and heat transfer encompassing the associated non-linearities.

Details of the PFBR core are discussed in the section *Details of the PFBR core*. The methodology

adopted for linear stability analysis is discussed in detail in the section *Linear stability analysis*, along with an estimation of the time constant and the establishment of stability through the Nyquist criteria. In the section *Reactivity perturbation study*, the response of the system with various reactivity perturbations is discussed. Point kinetics equations and heat transfer equations associated with the coolant channel are solved to get the time evolution of reactor power and temperatures.

It has to be noted that in thermal reactors, especially boiling water reactors (BWR), the stability of the system is of primary concern due to the presence of Xe and other poisons. The loosely coupled large cores of commercial thermal reactors make them vulnerable to unstable oscillations. Stable limit cycle oscillations are found in BWR at low-flow conditions. Compared to thermal reactors, fast reactors show good stability characteristics due to their tightly coupled core with strong negative reactivity feedback effects, coolant in single liquid phase and the lack of poison effects in the fast flux region.

### DETAILS OF THE PFBR CORE

PFBR is a 500 MW (electrical) MOX-fuelled fast reactor with two enrichment zones. Important core parameters pertaining to the reactor are given in tab. 1. 2-D diffusion theory calculations are performed using a ABBN cross-section set for calculating reactivity worth distributions and power densities which are essential for the stability studies discussed here.

\* Corresponding authors; e-mail: anuraj@igcar.gov.in

**Table 1. Liquid metal fast breeder reactor design parameters**

Thermal output [MW]	1250
Maximum linear heat rating [ $\text{Wm}^{-1}$ ]	$450 \cdot 10^2$
Active core height [m]	1
Number of sub-assemblies in core1/core2	85/96
Plutonium enrichment [%]	20.7/27.7
Fuel pins per sub-assembly	217
Assembly pitch [m]	0.135
Fuel pin diameter [mm]	6.6
Clad thickness fuel [mm]	0.45
Equivalent core diameter [m]	2
System pressure [MPa]	0.607
Total mass flow rate [ $\text{kgs}^{-1}$ ]	$6.959 \cdot 10^2$
Coolant inlet temperature [K]	670
Coolant outlet temperature [K]	833
Coolant inlet density [ $\text{gm}^{-3}$ ]	$8.423 \cdot 10^5$
Coolant heat capacity at $T$ [ $\text{Jkg}^{-1}\text{K}^{-1}$ ]	$1.268 \cdot 10^3$
Coolant thermal expansion coefficient [ $\text{K}^{-1}$ ]	$9.5 \cdot 10^{-3}$

Reactor kinetics parameters for the PFBR core are given in tab. 2.

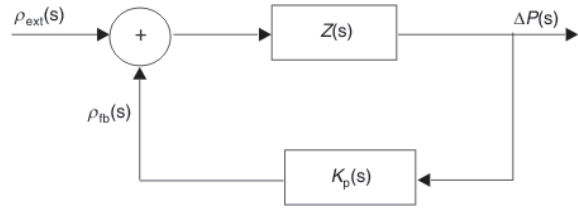
**Table 2. Kinetics parameters for PFBR**

Prompt neutron generation time, $\Lambda$ [s]	$4.1 \cdot 10^{-7}$					
Delayed neutron fraction, $\beta_{\text{eff}}$ [pcm]	355					
$j$	1	2	3	4	5	6
$\beta_j$ (pcm)	8.246	76.817	66.926	128.49	57.615	17.213
$\lambda_j$ [ $\text{s}^{-1}$ ]	0.01290	0.03120	0.13440	0.34480	1.3922	3.7491

For convenience, delayed neutron fractions are given in pcm units. It should be noted that  $1 \text{ pcm} = 1 \cdot 10^{-5} \Delta k/k$ .

## LINEAR STABILITY ANALYSIS

Point kinetics equations describing reactor kinetics are non-linear since the reactivity depends on the power. But for small perturbations, the stability of a non-linear system could be deduced from the stability of an associated linear system. In the present study, the equations of reactor dynamics are linearized around the equilibrium point and a linear stability analysis is carried out in terms of transfer functions. The block diagram representing the feedback loop in a reactor system is given in fig. 1. Block  $Z(s)$  is the forward-loop transfer function representing the point kinetics equations connecting power and reactivity. Block  $K_p(s)$  is the feedback transfer function calculated by solving the heat transfer equations and reactivity feedback relations. A system transfer function is defined as the ratio of Laplace transforms of the output parameter to the input parameter.

**Figure 1. Block diagram representing the reactor system**

here,  $Z(s)$  is known as the zero power transfer function and  $K_p(s)$  as the feedback transfer function. Out of this, the zero power transfer function can be obtained from point kinetics equations as

$$Z(s) = \frac{1}{s \Lambda \sum_{j=1}^6 \frac{\beta_j}{s + \lambda_j}} \quad (1)$$

where  $\Lambda$  is the prompt neutron generation time,  $\beta_j$  – the delayed neutron fractions of the six group,  $\lambda_j$  – the decay constants of delayed neutron precursor, and  $\omega$  – the cycles frequency

Mathematically, the dynamic power coefficient  $K_p(s)$ , also known as the reactivity feedback transfer function, is defined as the ratio of the Laplace transform of reactivity feedback  $\rho_{\text{fb}}(s)$  to the Laplace transform of change in power  $\Delta P(s)$  that is

$$K_p(s) = \frac{\rho_{\text{fb}}(s)}{\Delta P(s)} \quad (2)$$

where  $s$  is the Laplace transform variable. If  $s$  is replaced by  $i\omega$ ,  $\omega$  being the frequency in cycles per second (rps),  $K_p(i\omega)$  is the frequency response function. The frequency response function is of the form

$$K_p(i\omega) = \frac{\alpha}{1 + i\omega\tau} \quad (3)$$

where  $\alpha$  is the static power coefficient and  $\tau$  – the time constant of feedback.

The dynamic power coefficient of reactivity is calculated by solving the heat transfer equations applicable to the coolant channels in the frequency domain. The lumped model of heat transfer used in the methodology is described in detail in refs. [1, 2]. The basics are also well explained in [3].

In the reactor, during power perturbation, transient temperature changes are not immediate with the changes in reactor power. The temperature depends on the ratio of energy-to-heat capacity; hence, the change in temperature and the expansion effects will lag behind the change in power. In addition, the time required for the heat transfer across the channel also directly affects the reactivity feedback and, thereby, the kinetic behavior of the fast reactor. The feedback due to fuel and clad axial expansion, coolant expansion, spacer-pad expansion and the Doppler effect have also been considered. The feedback contribution from

blanket, differential control rod expansion and reactor vessel expansion were ignored because of their contribution, deemed small.

### Calculation method

Along with the radial and axial blankets, the core region is modeled in the analysis as well. The reactor is assumed to be divided into various radial zones/channels based on the flow zoning of the reactor. Since the power rating varies significantly axially, the core height is divided into several axial meshes. In the current study, the PFBR core is assumed to be divided into 10 radial and 14 axial zones. Each radial zone contains a certain number of subassemblies with identical coolant flow rates. It is assumed that in a particular radial zone all the fuel pins behave identically thermodynamically and, hence, heat transfer calculations are done only for a representative pin from each of the radial channels.

For computational simplicity, the dynamic reactivity coefficient  $K_p(i\omega)$  is written as

$$K_p(i\omega) = \Delta\rho^{j,i} \Delta T^{j,i}(i\omega) \quad (4)$$

where  $\Delta\rho^{j,i}$  is the isothermal temperature coefficient of reactivity and  $T^{j,i}(i\omega)$  represents the frequency-dependent temperature change per unit change in power. Superscripts  $j$  and  $i$  represent the axial and radial mesh numbers. The calculation of frequency-dependent temperature change  $T^{j,i}(i\omega)$  is discussed below. Reactivity feedbacks corresponding to this temperature change are calculated using the perturbation worth and expansion coefficients. Perturbation worths are calculated based on a 26-group ABBN cross-section set. Reactivity feedbacks from all the prominent feedback mechanisms are added to give the dynamic reactivity coefficient for that frequency, eq. (4).

### Calculation of frequency-dependent temperature rise $T^{j,i}(i\omega)$

A radially lumped axially continuous heat transfer model is employed for heat transfer calculations. In this model, heat transfer equations for fuel, clad, coolant and structural material are

$$C_f \frac{\partial T_f(z,t)}{\partial t} = \Psi(z)P(t) - h_f [T_f(z,t) - T_s(z,t)] \quad (5)$$

$$C_s \frac{\partial T_s(z,t)}{\partial t} = h_f [T_f(z,t) - T_s(z,t)] - h_s [T_s(z,t) - T_c(z,t)] \quad (6)$$

$$C_c \frac{\partial T_c(z,t)}{\partial t} = h_s [T_s(z,t) - T_c(z,t)]$$

$$C_{c,v} \frac{\partial T_c(z,t)}{\partial z} = h_{st} [T_c(z,t) - T_{st}(z,t)] \quad (7)$$

$$C_{st} \frac{\partial T_{st}(z,t)}{\partial t} = h_{st} [T_c(z,t) - T_{st}(z,t)] \quad (8)$$

where  $T$  is the temperature,  $\Psi(z)$  – the axial power distribution,  $P(t)$  – the reactor power per unit length,  $C$  – the heat capacity per unit length,  $h$  – the lumped heat transfer coefficient per unit length,  $v$  – the coolant velocity,  $t$  – the time, and  $z$  – the axial distance

Subscripts  $f$ ,  $s$ ,  $c$ , and  $st$  stand for fuel, stainless steel, coolant, and structural material (sheath), respectively.

Basically, eqs. (5) to (8) are non-linear. To solve them in the frequency domain, these equations are linearized. A small perturbation in reactivity is initiated which would lead to change in power and temperature, as follows

$$\begin{aligned} P(t) &= P_0 + \Delta P(t) \\ T_f(z,t) &= T_{f0}(z) + \Delta T_f(z,t) \\ T_c(z,t) &= T_{c0}(z) + \Delta T_c(z,t) \\ T_s(z,t) &= T_{s0}(z) + \Delta T_s(z,t) \\ T_{st}(z,t) &= T_{st0}(z) + \Delta T_{st}(z,t) \end{aligned} \quad (9)$$

where  $\Delta$  represents the small perturbation. For a step change in power at time  $t = 0$ ,  $\Delta P(t) = \Delta P = P_1 - P_0$  for all  $t$ , where  $P_1$  and  $P_0$  are the final and initial powers.

Substituting eq. (9) into eqs. (5) to (8) and solving them after taking the Laplace transform with constant inlet temperature assumption we get

$$\Delta T_c(z,s) = \frac{\Delta P e^{-z/v}}{h_s(1 - s\tau_f)\tau_3 v \tau_c} \int_0^z \Psi(z') e^{s z'/v} dz' \quad (10)$$

$$\Delta T_s(z,s) = \frac{\Psi(z)\Delta P}{h_s(1 - s\tau_f)\tau_3} \frac{\Delta T_c(z,s)}{\tau_3} \quad (11)$$

$$\Delta T_f(z,s) = \frac{\Psi(z)\Delta P}{h_f(1 - s\tau_f)} \frac{\Delta T_s(z,s)}{(1 - s\tau_f)} \quad (12)$$

where  $s$  is the Laplace transform variable, and

$$\begin{aligned} \tau_3 &= \frac{1 - s\tau_s}{h_s} \frac{h_f}{h_s} \frac{1}{1 - s\tau_f} \\ \tau &= \frac{1 + s\tau_c}{h_s} \frac{h_{st}}{h_s} \frac{s\tau_{st}}{1 - s\tau_{st}} \frac{1}{\tau_3} \\ \tau_f &= \frac{C_f}{h_f}, \tau_s = \frac{C_s}{h_s}, \tau_c = \frac{C_c}{h_s}, \text{ and } \tau_{st} = \frac{C_{st}}{h_{st}} \end{aligned}$$

where  $\tau_f$ ,  $\tau_s$ ,  $\tau_c$ , and  $\tau_{st}$  are the time constants of fuel, steel (clad), coolant, and structural material. For sufficiently small changes in power and reactivity, nonlinear effects in heat transfer equations can be neglected. Therefore, terms with products of small quantities are ignored.

For numerical calculation, the core is divided into axial and radial zones. Substituting  $s$  with  $i\omega$ , the above equations become

$$\Delta T_c(j, i, i\omega) = \frac{e^{\frac{\tau z(j)}{\nu(i)}}}{h_s(1 - i\omega\tau_f)\tau_3\nu(i)\tau_c} \prod_{j=1}^j (P_2 - P_1)\Psi(j, i) \frac{\nu(i)}{\tau} e^{\frac{\tau z(j-1)}{\nu(i)}} e^{\frac{\tau z(j)}{\nu(i)}} \quad (13)$$

$$\Delta T_s(j, i, i\omega) = \frac{\Psi(j, i)(P_2 - P_1)}{h_s\tau_3(1 - i\omega\tau_f)} \frac{\Delta T_c(j, i, i\omega)}{\tau_3} \quad (14)$$

$$\Delta T_f(j, i, i\omega) = \frac{\Psi(j, i)(P_2 - P_1)}{h_f(1 - i\omega\tau_f)} \frac{\Delta T_c(j, i, i\omega)}{1 - i\omega\tau_f} \quad (15)$$

where  $\omega$  is the angular frequency. The  $j$  and  $i$  are the axial and radial mesh indices.

The feedback reactivity components are computed in the frequency domain by computing the material expansion with the change in temperature and thermal expansion coefficient, and then multiplied with reactivity worth.

**RESULTS**

The magnitude and phase of the feedback transfer function are shown in figs. 2 and 3.

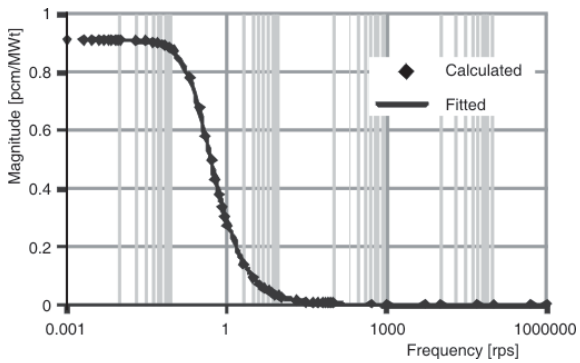


Figure 2. Magnitude of feedback transfer function

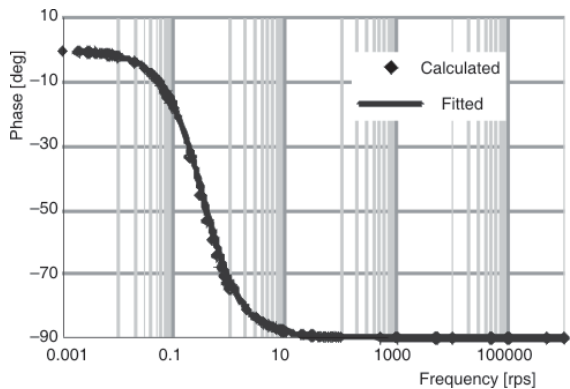


Figure 3. Phase of feedback transfer function

The time constant is found to be 3.05 s [1] by fitting the calculated profile of the feedback reactivity transfer function with the expression (3), figs. 2 and 3.

A necessary but not sufficient condition for stability is that  $K_p(0) < 0$ , i. e. that the static power coefficient of the reactor must be negative. The static power coefficient of reactivity for PFBR is  $-0.699$  pcm/MW (0 to 100 % power) and  $-0.794$  pcm/MW (0 % to 50 % power). Thus, the necessary condition of stability is satisfied [3].

A necessary and sufficient condition for stability is expressed in terms of the open-loop reactor transfer function which is defined as

$$L(i\omega) = P_0 Z(i\omega) K_p(i\omega) \quad (16)$$

where  $P_0$  is the steady-state power and  $Z(i\omega)$  is the zero power frequency response function of the reactor.

The open-loop transfer function is derived from the expression of the power transfer function which is defined as

$$H(i\omega) = \frac{P_0 Z(i\omega)}{[1 - P_0 Z(i\omega) K_p(i\omega)]} \quad (17)$$

The magnitude and phase of the zero power transfer function and the power transfer function are plotted in figs. 4 and 5.

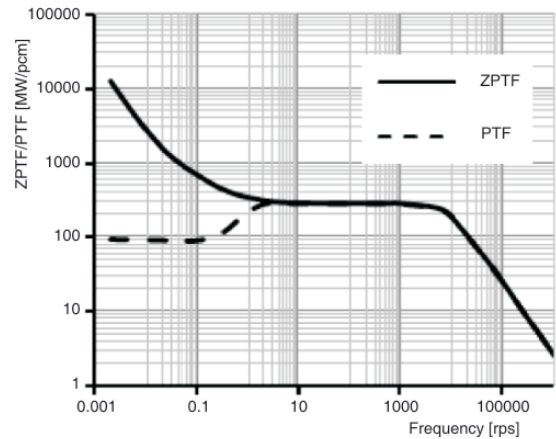


Figure 4. Magnitude of zero power transfer function and power transfer function (1 rps = 6.283 radians/second)

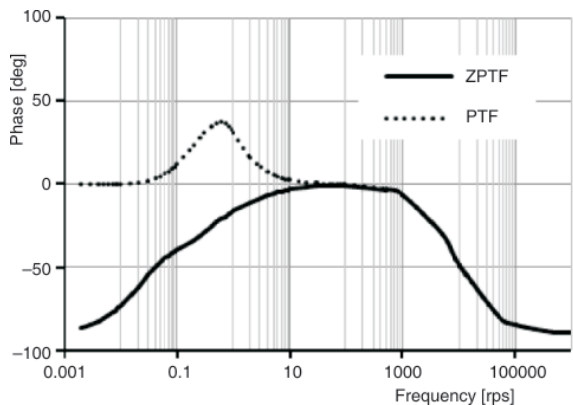


Figure 5. Phase of zero power transfer function and power transfer function

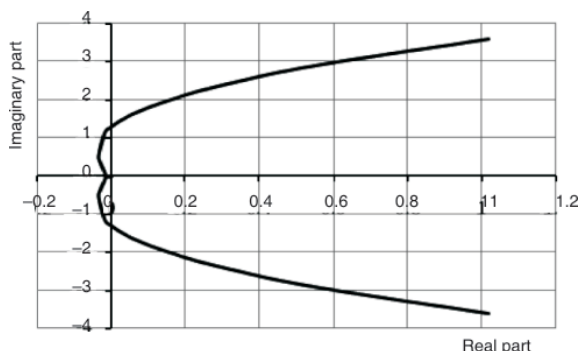


Figure 6. Nyquist plot for PFBR

Real and imaginary parts of  $L(i\omega)$  are plotted against each other to get the Nyquist plot. If the curve encircles the  $(-1, 0)$  point, then the reactor is unstable. Otherwise, the reactor is stable [3].

The Nyquist plot for PFBR is given in fig. 6. It can be seen that the curve is far away from the  $(-1, 0)$  point, confirming that the PFBR is stable. Important thermophysical parameters used for estimating the feedback reactivity transfer function and kinetics parameters applied in the estimation of the zero power transfer function are given in tabs. 1 and 2.

### REACTIVITY PERTURBATION STUDY

While the Nyquist criteria establish the inherent stability of a reactor, a direct verification of power evolution for various reactivity perturbations and at various power levels of reactor operation offers fullproof evidence of reactor stability at said input perturbations. The power should converge in few seconds and should not have major oscillations. Reactivity pulse perturbations were the input for various reactivity pulses and at various power levels. The power comes back to the nominal value without any oscillations. To check reactor stability when the reactivity input is oscillatory in nature, reactor power, fuel temperature and coolant temperature evolution have been checked for sinusoidal input with various frequencies and with different reactivity feedback conditions.

#### Step reactivity insertions

The stability of the PFBR has been checked against a small reactivity perturbation of 0.1  $\$$  and large reactivity perturbations of 0.3  $\$$  and 0.5  $\$$ . It should be noted that the reactivity unit  $\$$  is a system-dependent unit equal to the effective delayed neutron fraction  $\beta$  (that is  $1 \$ = 1/\beta \text{ } k/k$ ). If the reactivity is greater than 1  $\$$ , the reactor will be super prompt critical. Reactivity perturbations are of one second duration and an input from 10 s to 11 s in the steady-state, starting from time zero. The study is done for full power and, also, part-load operation of 40 % power

and 20 % power with an appropriate lower coolant flow of 59.8 % and 50 %. The large but unlikely reactivity perturbation of 1  $\$$  (prompt critical) is also studied. Apart from the reactivity perturbation, a flow perturbation of 10 % at full power is studied as well.

The analysis is carried out with the transient analysis code PREDIS which is a part of the KALDIS code system [4]. The reactivity pulse input is between 10 s and 11 s, the reactivity input remaining zero at all other times. The kinetics portion of the PREDIS code has been validated against SEFOR experiments and FBTR reactivity transients [5, 6]. The processes modeled in the code are neutronics, transient thermal hydraulics, reactivity feedbacks such as Doppler, fuel and clad axial expansion, coolant expansion, spacer pad, grid plate, main vessel and differential control rod expansion, coolant boiling, clad and fuel melting and slumping. A detailed description of the mathematical modeling for reactor kinetics and thermal hydraulics is given in [4]. In the calculations presented, the lumped model of heat transfer adapted for analysis of unprotected transients is employed. The same model was applied for linear stability analysis of the PFBR [1]. The exact heat conduction model, which takes into account temperature dependent thermal conductivity, is employed for the analysis of protected transients. In the present study, the reactor does not SCRAM when the reactivity perturbation is input and, thus, the plant protection system (PPS) is assumed not to be functional.

Reactivity perturbations input pulses are taken for the duration of 1s. This is appropriate in this analysis, since the time constant of reactivity feedback for the core is 3.05 s [1] and the duration of 1 s is a good compromise to study feedback reactivity and power evolution. A shorter perturbation will give a benign effect and a longer duration will be a problem for safety analysis (not a perturbation). The reactivity values are chosen so as to represent small and large values. 0.1  $\$$  (33.7 pcm) is considered a small pulse, though it is conservative in that. The sodium-removal worth of the central subassembly is +17 pcm. The removal of sodium from the entire central subassembly is an unlikely occurrence. Higher values of 0.3  $\$$  and 0.5  $\$$  have been considered in this analysis. These are large perturbations unlikely to occur. For the sake of illustration, an unlikely large perturbation leading to prompt critical (1  $\$$ ) has also been considered. The range of reactivity perturbations considers the entire possible range and this analysis is adequate to establish the stability of the reactor.

The results of the analysis of some reactivity perturbations are given graphically for the various cases. Figures 7 and 8 give the evolution of net reactivity and normalized power for reactor operation at full power and for reactivity perturbation inputs of 0.1  $\$$  and 0.5  $\$$ . Figures 9, 10, and 11 give the evolution of net reactivity and normalized power for part-load operation of 20 % power (50 % flow) for reactivity pulses of 0.1  $\$$ , 0.3  $\$$ , and 0.5  $\$$ .

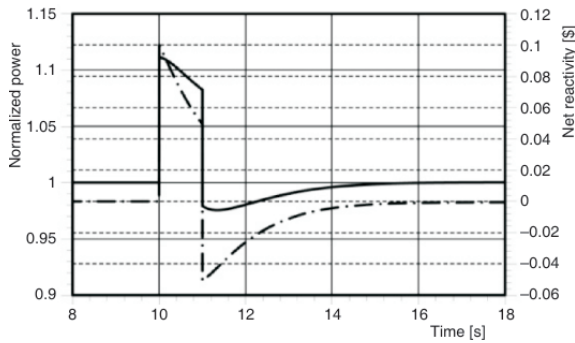


**Figure 7. Net reactivity and normalized power with time; power = 100 %, flow = 100 %, perturbation = 0.1 \$**  
Normalized power      Net reactivity

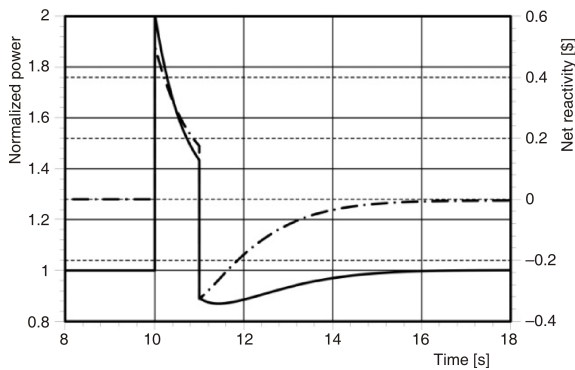


**Figure 8. Net reactivity and normalized power with time; power = 100 %, flow = 100 %, perturbation = 0.5 \$**  
Normalized power      Net reactivity

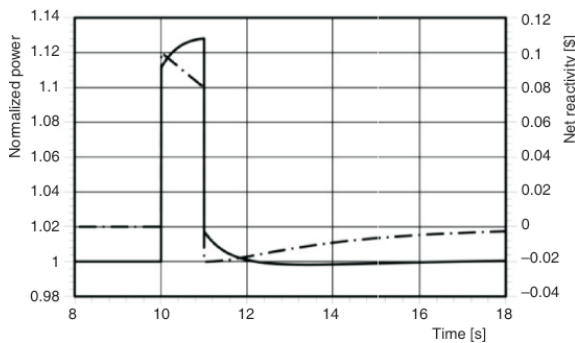


**Figure 9. Net reactivity and normalized power with time; power = 20 %, flow = 50 %, perturbation = 0.1 \$**  
Normalized power      Net reactivity

A careful observation of reactivity inputs of 0.1 \$, 0.3 \$, and 0.5 \$ brings out the fact that power converges to the original steady-state value in a few seconds, without any oscillation. Table 3 gives the times taken for the power to stabilize to the original value. The power is steady after reaching its original value. As the value of reactivity perturbation is higher, the peak power reached is also higher, as expected. For a 100 % power (and 100 % flow), the power reaches peak value of 111 % and 200 % for 0.1 \$ and 0.5 \$, respectively, figs. 7 and 8. When the power level is low, reactivity feedbacks are lower. Hence, for lower power levels, the neg-

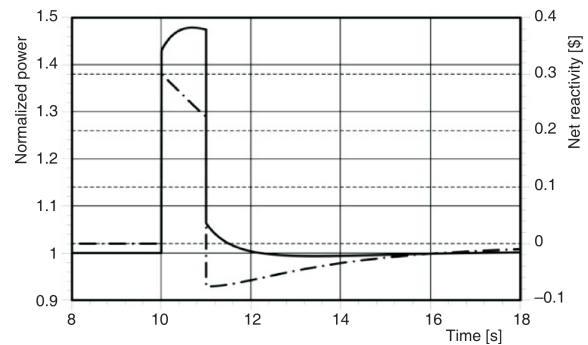


**Figure 10. Net reactivity and normalized power with time; power = 20 %, flow = 50 %, perturbation = 0.3 \$**  
Normalized power      Net reactivity

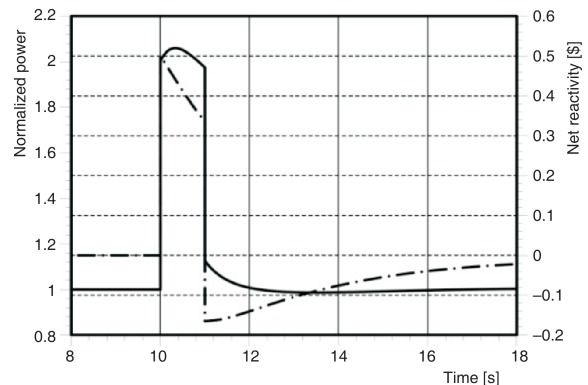


**Figure 11. Net reactivity and normalized power with time; power = 20 %, flow = 50 %, perturbation = 0.5 \$**  
Normalized power      Net reactivity

ative reactivity reached is lower. As illustration, in case of a 0.5 \$ perturbation, the negative reactivities reached are -0.32 \$ and -0.17 \$ for 100 % power (100 % flow) and 20 % power (50 % flow), respectively, figs. 8 and 11.

The behaviour of major feedbacks is illustrated in fig. 12 for the case of 20 % power (50 % flow) with 0.3 \$ input perturbation. The Doppler, fuel expansion and spacer pad expansion feedbacks, which are the major feedbacks, have been plotted. All these are negative in these perturbations, with Doppler being most negative followed by fuel expansion and spacer pad expansion. For illustration, a case of flow perturbation has also been analysed. A perturbation of 10 % increase in flow value is input for one second (10 s to 11 s). At all other times flow is nominal and reactivity is zero. The results for evolution of normalised power and net reactivity is given in fig. 13. It can be seen that the power rises to a low value of 100.2 % then falls down and returns to initial value at 15.5 s. The reactivity feedbacks in this case are depicted in fig. 14.

### Sinusoidal reactivity insertions

The stability of the PFBR has also been checked with sinusoidal reactivity perturbations of an ampli-

**Table 3. Time taken for power to reach original steady-state value for the various reactivity perturbations**

No.	Power [%]	Flow [%]	Reactivity perturbation input between 10 s and 11 s	Time at which reactor comes to original steady-state power level (s)	Time taken after the perturbation to reach original steady-state (s)
1	100	100	0.1	16.6	5.6
2	100	100	0.3	16.8	5.8
3	100	100	0.5	16.9	5.9
4	40	59.8	0.1	18.2	7.2
5	40	59.8	0.3	18.3	7.3
6	40	59.8	0.5	18.3	7.3
7	20	50	0.1	16.89	7.89
8	20	50	0.3	16.90	7.90
9	20	50	0.5	16.90	7.90

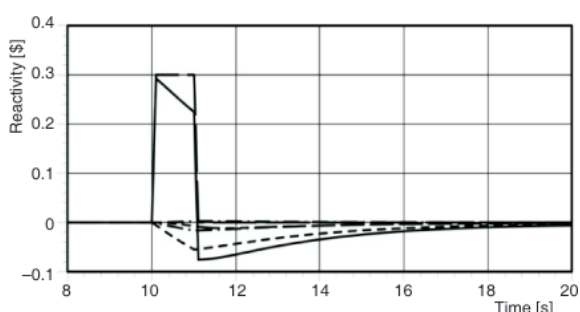


**Figure 12. Input reactivity, net reactivity and reactivity feedbacks; power=20 % flow=50 %, perturbation=0.3 \$**  
 — Input, - - - Steel expn, . . . . Spacer pad, - . - . Net, . . . . Fuel expn., . . . . Sodium expn. - - - - Doppler

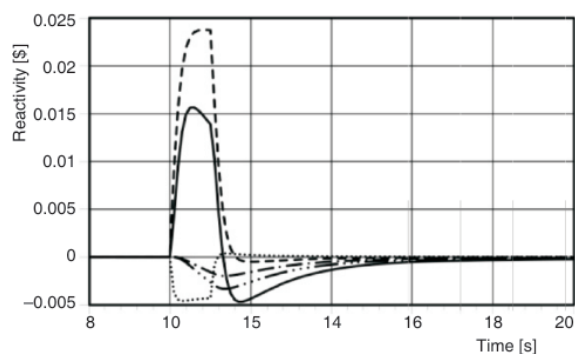


**Figure 14. Input reactivity, net reactivity and reactivity feedbacks, power = 100 %, flow perturbation 10 %**  
 — Net, - - - - Doppler, . . . . Sod. expn., - . - . Spacer pad, - - - - Fuel expn

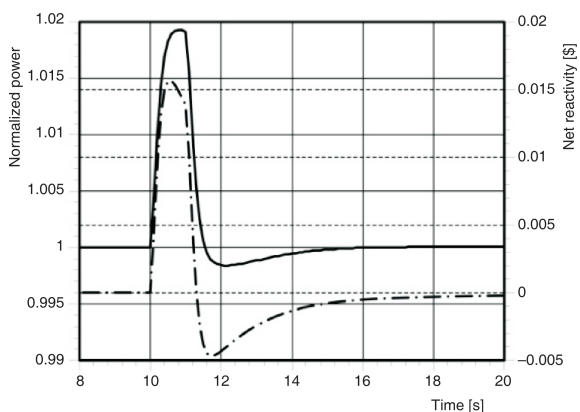


**Figure 13. Net reactivity and normalized power with time; power = 100 %, flow perturbation 10 %**  
 Normalized power Net reactivity

tude of 0.5 \$ and frequencies of 10 Hz, 1 Hz, 0.1 Hz, and 0.01 Hz, by considering all reactivity feedbacks and, also, by ignoring all reactivity feedbacks. The reactor is stable when all reactivity feedbacks are included. The reactor is stable when the Doppler feedback alone is considered, as well. When all feedbacks are excluded, the power increases with time and fuel temperature reaches the melting point. The increase is greater for low frequencies, thus indicating that the reactor becomes unstable at low frequencies, when all

feedbacks are suppressed. Computer code PREDIS [4] has been used for the transient analysis with the sinusoidal reactivity input. A lumped model of heat transfer has been employed in the present analysis.

Some results of the analysis presented here are given in the form of graphs which give the variation of normalized power, peak fuel temperature and peak clad (steel) temperature with time. In all cases, the duration of 50 cycles for the sinewave has been considered to precisely check the dependence on frequency. Hence, the duration of the plot is different for each frequency.

Figure 15 gives the variation of the normalized power, peak fuel temperature and peak clad (steel) temperature, along with the time for the 10 Hz frequency, with/without reactivity feedbacks. The duration for 50 cycles (5 s) has been shown. It can be seen that when all reactivities are considered, the trend of mean normalized power is uniform. In the beginning, it goes down a little over a small duration of time, because fuel and steel temperatures have a small buildup time and, hence, the associated reactivity feedbacks. Fuel and clad temperatures saturate around 2261 K and 885.6 K and remain well below their melting points (3023 K for fuel and 1700 K for clad). When the reactivity feedbacks are suppressed, we see a monotonically increasing trend for normalized power, fuel temperature and

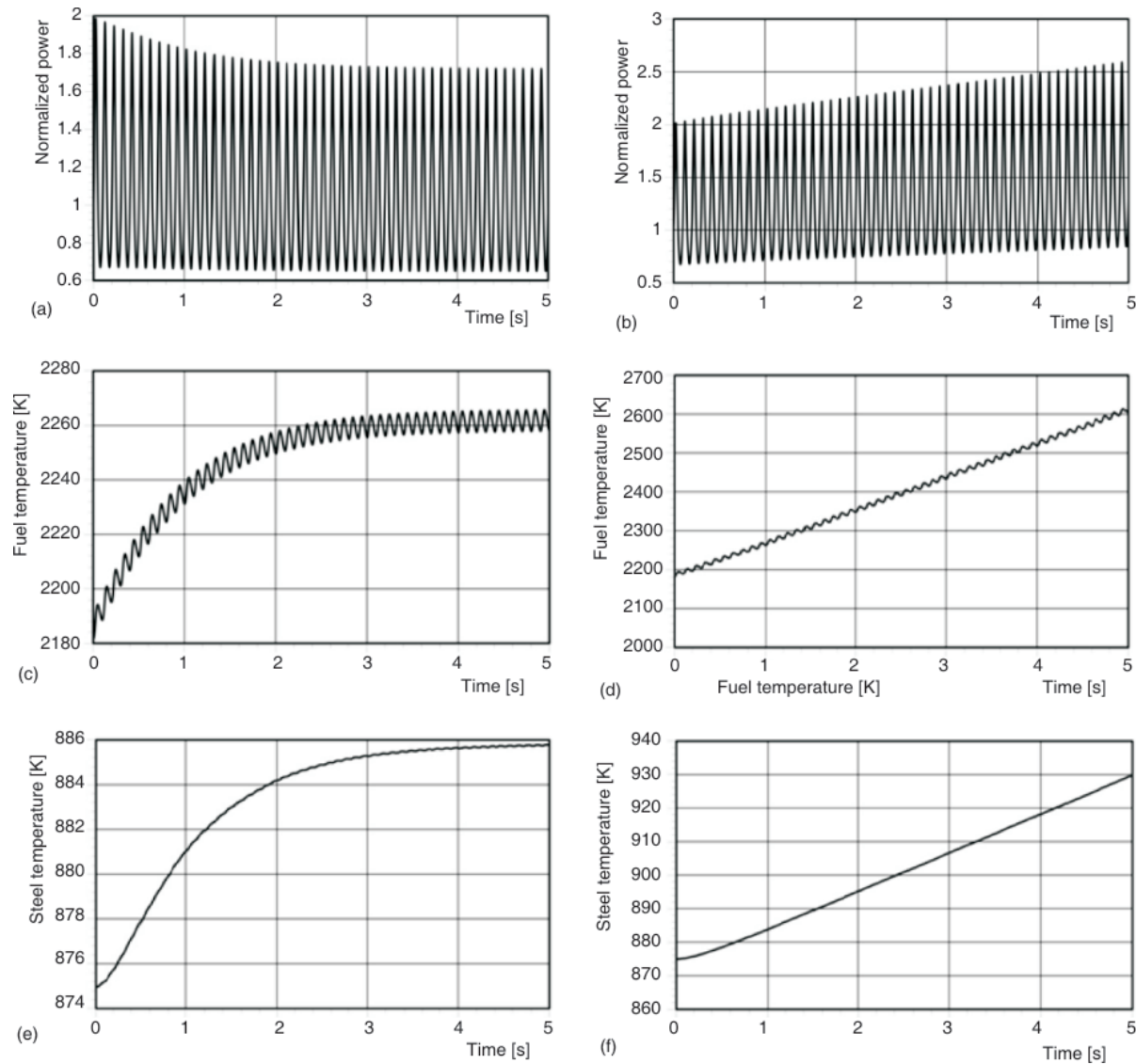


**Figure 15.** Normalized power, fuel temperature and steel temperature with time for sinusoidal input of 0.5 \$ amplitude, with (a, c, e) and without (b, d, f) reactivity feedback; frequency = 10 Hz

steel temperature. A more continuous evolution will lead to fuel and clad melting. Within the first 50 cycles (5 s), they remain below melting points, the peak fuel temperature being 2610 K and peak clad temperature being 930 K.

Figure 16 gives the variation of normalized power, peak fuel temperature, and peak clad (steel) temperature with time for the 0.01 Hz frequency, with reactivity feedbacks and without reactivity feedbacks. The duration for 50 cycles (5000 s) has been shown. It can be seen that when all reactivities are considered, the trend of mean normalized power is uniform. In the beginning, it goes down a little over a small duration of time because expansion feedbacks have a build up time. But this is not visible in the graph because it has been plotted for a long duration (5000 s). Fuel and clad temperatures saturate around 2200 K and 879 K, and remain well below their melting points (3023 K for

fuel and 1700 K for clad). When the reactivity feedbacks are suppressed, we see a monotonically increasing trend for normalized power, fuel temperature and steel temperature. The normalized power goes up, and fuel reaches the melting point at 8.4 s.

A case excluding all expansion feedbacks and retaining only the Doppler feedback has also been studied. Figure 17 shows the result of this study for the frequency of 10 Hz to 0.01 Hz. The duration for 50 cycles (5 s for the frequency of 10 Hz and 5000 s for the frequency of 0.01 Hz) are shown. It can be seen that the trend of mean normalized power is uniform. There is a small buildup time for fuel and steel temperature and, hence, they initially go up and, upon this, saturate. Accordingly, the Doppler feedback also initially changes, eventually to be reflected by the decreasing profile of the normalized power at the beginning of the 10 Hz frequency. As for the case of 0.01 Hz, this is

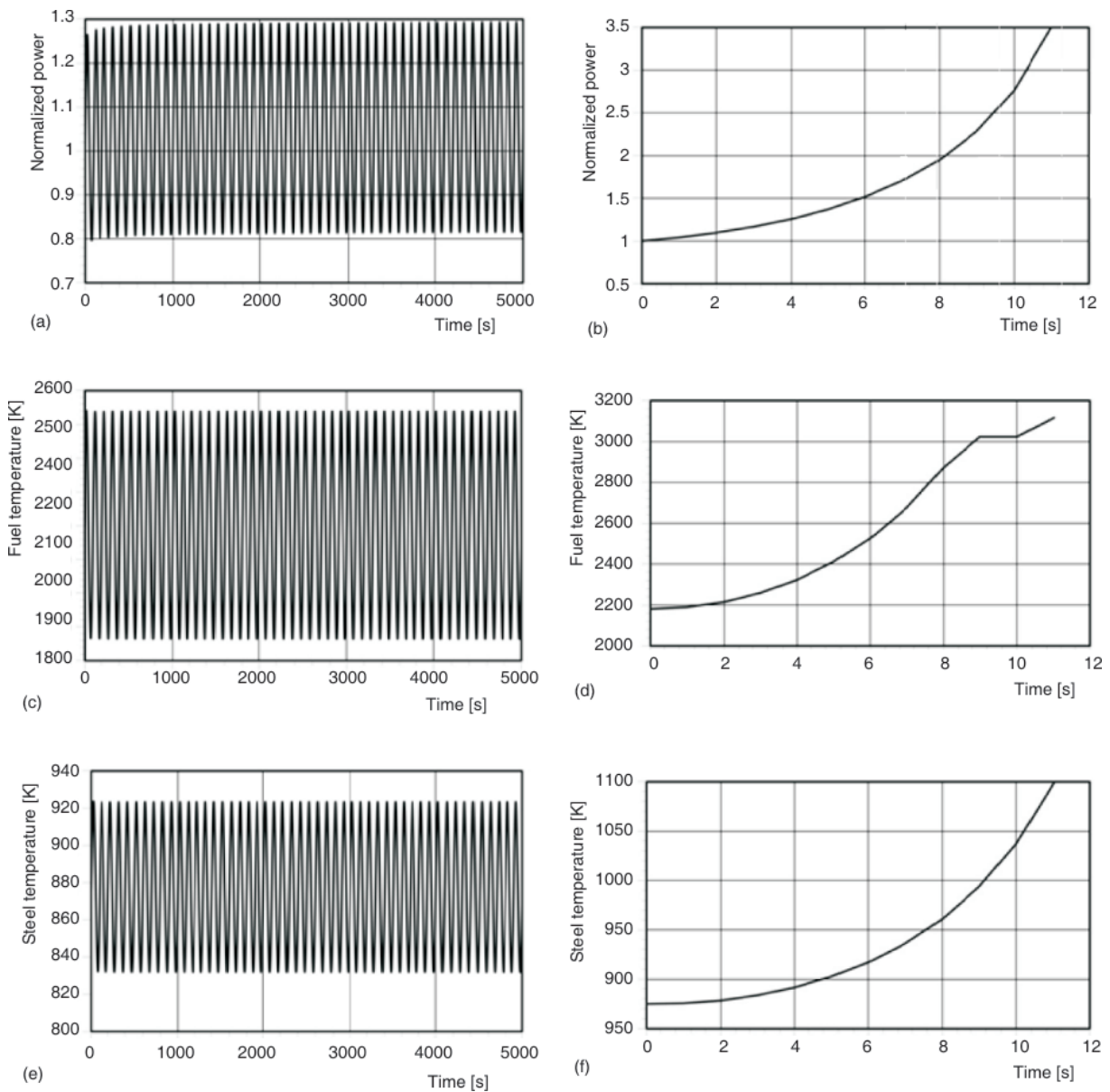


**Figure 16. Normalized power, fuel temperature and steel temperature with time for sinusoidal input of 0.5 \$ amplitude, with (a, c, e) and without (b, d, f) reactivity feedback; frequency = 10 Hz**

not visible, since the plot spans a much longer time (5000 s). The peak fuel and clad temperatures lie below their melting points in both cases (2325 K for 10 Hz, 2300 K for the 0.01 Hz fuel, 893 K for 10 Hz, 890 K for 0.01 Hz for clad). Hence, the reactor is stable with Doppler feedback alone.

### CONCLUSION

The stability of a medium-sized FBR core has been studied thoroughly by linear stability analysis and, also, with reactivity perturbations in the form of pulses and sine waves. Linear stability gives a nega-

tive dynamic power coefficient with the time constant of 3.05 s meeting the necessary condition for stability. The Nyquist plot of the loop transfer function does not encircle  $(-1, 0)$  point in the complex plane, thus meeting the necessary and sufficient conditions for stability. The analysis with a complete range of reactivity perturbations in the form of pulses indicates that reactor power comes back to the nominal value without any oscillation, proving the strong stability of the reactor. Analysis with sinusoidal pulses of various frequencies indicates that the reactor is stable in the strong sense when all reactivity feedbacks are considered and even when the Doppler feedback alone is considered.

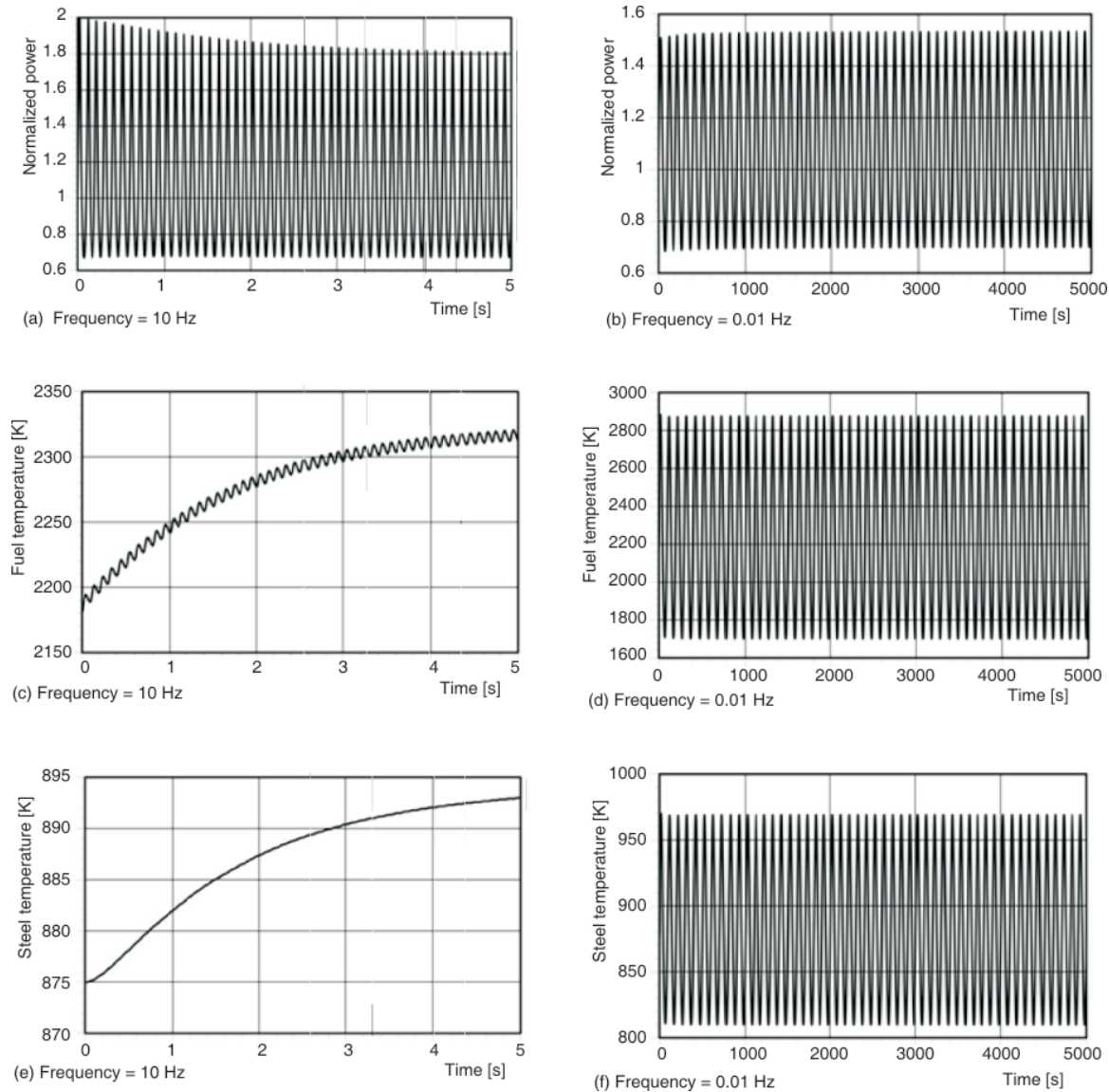


**Figure 17. Normalized power, fuel temperature and steel temperature with time for 10 Hz (a, c, e) and 0.01 Hz (b, d, f) with Doppler feedback alone**

#### AUTHOR CONTRIBUTIONS

Linear stability analysis using the Nyquist criteria was performed by V. L. Anuraj, while the transient analysis with reactivity perturbations was done by G. S. Srinivasan. K. Devan provided overall guidance during the study, interpreting the results and providing the necessary input required for the calculations. The analysis of results and preparation of the manuscript was a joint undertaking of all authors mentioned.

#### REFERENCES

- [1] Anuraj, V. L., Srinivasan, G. S., Dynamic Power Coefficient of Reactivity Calculations and Stability Analysis with Perturbation Worths Based on ABBN 93 cross section set, 19<sup>th</sup> National Symposium on Radiation Physics, Chennai, Tamil Nadu, India, 2012

- [2] Singh, O. P., *et al.*, Response to Small Reactivity Perturbations in an Oxide and Metal Fuelled Medium-Sized Liquid-Metal Fast Breeder Reactor, *Annals of Nuclear Energy*, 20 (1993), 5, pp. 315-319
- [3] Hummel, H. H., Okrent, D., Reactivity Coefficients in Large Fast Power Reactors – ANS Publication, USA, 1979, p. 386
- [4] Harish, R., *et al.*, KALDIS: A Computer Code System for Core Disruptive Accident Analysis in Fast Reactors, IGCAR Report, IGC-208, 1999
- [5] Sharada, B., Singh, O. P., Validation of the Computer Code, POKIN against SEFOR Experiment and Analytical Results, IGCAR Report ROD/01117/SNAS-32, 1990
- [6] Srinivasan, G. S., Singh, O. P., Validation of the Computer Code, PREDIS Against FBTR Experimental Reactivity Transients, IGCAR Report RPD/SAS/FBTR/01100/CR/011, 1999

Paper on April 27, 2015

Accepted on May 15, 2015

**Виџајан Л. АНУРАЦ, Говерапет С. СРИНИВАСАН, Кунхираман ДЕВАН**

**СВОЈСТВА СТАБИЛНОСТИ ИНДИЈСКОГ ПРОТОТИПА  
БРЗОГ РЕАКТОРА СНАГЕ ОД 500 MW**

По истеку више од две деценије успешног деловања брзог оплодног тест реактора, Индија је данас близу завршетка прототипа брзог оплодног реактора снаге 500 MW електричних. Овај брзи реактор базенског типа, са снагом за комерцијалну употребу, хлађен је натријумом и пуњен мешаним оксидним горивом. Својства стабилности реактора представљају значајне сигурносне аспекте који се проучавају. У овом раду, спроведена је линеарна анализа стабилности прототипа брзог оплодног реактора методом преносне функције, док је стабилност система проверена Никвистовим критеријумом. У циљу комплетирања проучавања, извршена је анализа транзијената са различитим врстама пертурбација реактивности. Одзив система такође је указао да је систем стабилан.

*Кључне речи: брзи оплодни реактор са течним металом, линеарна стабилност, прототипни брзог оплодног реактора, Никвистов дијаграм*

---